EXTENDED EXPERIMENTAL PROCEDURES

Protein expression and purification

GluR6 and KA2 ATD constructs with native signal peptides were cloned into the pRK5-IRES-EGFP expression vector with a C-terminal LELVPRGS-His_8 affinity tag and thrombin cleavage site as described previously (Kumar and Mayer, 2010; Kumar et al., 2009). Mutants were prepared by overlap PCR and the amplified regions sequenced on both strands. HEK293T and HEK293 cells lacking N-acetylglucosaminyltransferase I ($GnTI^-$) grown as adherent monolayer cultures were transiently transfected with plasmid DNA using the "PEI-MAX" form of polyethyleneimine (Polysciences, Inc Warrington, PA). We also used HEK293T and HEK293 $GnTI^-$ suspension cultures at a cell density of 15-2.0 million cells/ml grown in 500 ml Freestyle medium (Invitrogen), supplemented with 2% (v/v) fetal bovine serum, 2 mM L-glutamine, 100 units/ml Penicillin and 100 μg/ml streptomycin. The conditioned media was harvested 5-8 days after transfection for purification of the secreted glycoproteins and centrifuged at 4,000 rpm to remove cell debris. Tris-HCl (pH 8.0) and NaCl were added from 1 and 5M stock solutions to final concentrations of 50 and 200 mM, respectively; the volume was reduced by ultrafiltration (Millipore Labscale TFF system, Pellicon Ultracel 10 kDa), and the concentrate clarified by centrifugation at 40,000 rpm for 20 minutes at 4 ºC before loading onto a Ni^{2+} charged 1 ml HiTrap chelating HP column (Amersham). ATD proteins were eluted using a linear gradient of imidazole and the pooled fractions were dialyzed extensively against 20 mM HEPES pH 7.4, 0.2 M NaCl and 1mM EDTA. To remove the affinity tag, $CaCl_2$ was added to a final concentration of 10 mM and the protein was digested with thrombin at a 1:400 w:w ratio (Enzyme:Protein) at 25 °C for 90 minutes. The thrombin-digested

protein was dialyzed overnight against a buffer containing 20 mM sodium acetate, 200 mM NaCl & 1 mM EDTA, pH 5.0, and for proteins used for crystallization, subsequently digested with Endo H prepared in house at a 1:10 w:w ratio (Enzyme:Protein) for 120 minutes at 25 °C to trim N-linked glycans. The proteins were then further purified by cation exchange chromatography on an SP Sepharose column and analyzed for homogeneity using 20% SDS-PAGE. Purified protein was concentrated by shock elution from an SP Sepharose ion-exchange column, dialyzed against crystallization buffer containing 20 mM sodium acetate, pH 5.0, 200 mM NaCl, 1 mM EDTA, flash frozen in liquid nitrogen at 2 mg/ml and stored at –80 ºC.

Crystallization

Purified proteins were mixed with high throughput screens using a nanolitre pipetting robot (Mosquito, TTP, LabTech) and setup in 96 x MRC 3 well crystallization plates (Swissci). Sitting drops of 0.1 µl protein were mixed 1:1 with reservoir solution and equilibrated against 45 µl of reservoir solution at 20°C. Potential hits were then optimized in 24 well plates (Hampton Research) by the hanging drop vapor diffusion method at 20°C with 1µl protein solution mixed with 1µl well solution and 500 µl reservoir solution, with the exception of the GluR6Δ1 homodimer for which crystals were taken directly from 96 well trays. The reservoir for the GluR6Δ1 homodimer was from well D6 of the MORPHEUS protein crystallization screen (Gorrec, 2009), and contained 10% PEG 8K, 20% ethylene glycol, 0.02 M each 1,6-hexanediol, 1-butanol, (RS)-1,2-propanediol, 2-propanol, 1,4-butanediol, 1,3-propanediol, and 0.1 M MOPS/HEPES-Na pH 7.5; the mother liquor was used for flash freezing in liquid nitrogen with no additional cryoprotectant. For crystallization of the heterodimer, purified GluR6Δ1 and KA2

proteins were mixed in a 1:1 ratio (v/v) at a concentration of 2 mg/ml; the reservoir solution contained 0.15M $(NH_4)_2SO_4$, 18% PEG 4K, 0.1 M Tris pH 8.2. For crystallization of the heterotetramer a 1:1 mixture of the wtGluR6 and KA2 ATDs was purified by size exclusion chromatography, and the peak corresponding to the tetramer complex was concentrated to 2mg/ml; the reservoir contained 10% ethylene glycol, 5% PEG 8K and 0.1 M HEPES pH 8.0. Crystals were cryoprotected by serial transfer into mother liquor supplemented with increasing amounts of glycerol, to a final concentration of 15%, and flash frozen in liquid nitrogen.

Structure solution and refinement

GluR6Δ1 homodimer crystals belonged to space group I4 with cell parameters $a = b$ =191.8 Å, c = 47.0 Å and $\alpha = \beta = \gamma = 90°$. GluR6Δ1/KA2 heterodimer crystals belonged to space group $P2_12_12_1$ with cell parameters a = 65.6 Å, b = 139.5 Å, c = 195.4 Å and $\alpha = \beta = \gamma = 90°$. The GluR6wt/KA2 heterotetramer crystals belonged to space group C2 with cell parameters a = 365.9 Å, b = 109.0 Å, c = 155.0 Å and $\alpha = \gamma = 90°$, $\beta = 97.6°$. None of the datasets showed twinning as analyzed by Phenix xtriage (Adams et al., 2010). The GluR6Δ1 homodimer solution contained 2 monomers in the asymmetric unit assembled as a dimer (Matthews coefficient 2.3, solvent content 48%). The rotation (RFZ) and translation function (TFZ) scores were 12.4, 22.0 and 16.8, 49.1 respectively. The molecular replacement solution for GluKΔ1/KA2 heterodimer contained 4 monomers in the asymmetric unit assembled as two heterodimers, corresponding to a solvent content of 49% (Matthews coefficient 2.4). The RFZ scores were 8.4, 7.8, 7.4 and 7.7 and the TFZ scores 17.6, 29.4, 38.4 and 36.3 for the four protomers. Refined GluR6Δ1/KA2 heterodimer coordinates were used as search probes for molecular

replacement to solve the GluR6wt/KA2 heterotetramer structure. PHASER found 5 heterodimers (Matthews coefficient 3.2, solvent content 62 %) in the asymmetric unit. The RFZ and TFZ values were 18.4, 21.9, 17.7, 43.6, 20.8 and 64.8, 24.9, 86.7, 11.8, 54.3.

Simulated annealing was used as an initial procedure in crystallographic refinement to remove model bias. TLS groups were identified by motion determination analysis (Painter and Merritt, 2006). The heterotetramer structure was initially refined using the low resolution refinement protocol including a deformable elastic network (DEN) model as implemented in CNS 1.3 (Schroder et al., 2010). A GluR6/KA2 tetramer model was used as a reference to generate DEN restraints using default parameters. Calculations with MOLPROBITY (Davis et al., 2004) revealed that 94.0%, 96.7% and 88.7% of residues were in the preferred regions of the Ramachandran plot (Ramachandran et al., 1963) for the homodimer, heterodimer and heterotetramer structures respectively. The all atom clash scores were 8.9, 6.6 and 6.42 placing the structures in the 97^{th}, 100^{th} and 100^{th} percentile (with 100^{th} the best) of structures solved at resolutions of 2.74-3.24, 2.66-3.16 and 3.25-4.19 Å, respectively. Similarly, the MolProbity protein geometry scores were 1.9, 1.8 and 1.9 for the three structures placing them in 99^{th}, 100^{th} and 100^{th} percentile. Solvent accessible surface area was calculated using the CCP4 program areaimol; additional crystallographic calculations were performed using CCP4(CCP4, 1994) and the USF suite (Kleywegt et al., 2001). Figures were prepared using PyMol 1.3 (Schrödinger, LLC.).

Sedimentation analysis

The density and viscosity of the buffer used for AUC was measured using a DMA5000 densimeter and an AMVn automated micro viscometer (both Anton Paar, Austria), respectively. The protein partial specific volumes were determined using SEDNTERP (kindly provided by Dr. John Philo) with corrections for contribution of carbohydrates (Durchschlag, 1989). The molar interference signal increment as well as the extinction coefficients at 230 nm and 250 nm were determined from a multi-signal analysis on the basis of the theoretical extinction coefficient at 280 nm predicted from the amino acid composition.

SV experiments were carried out using 3 mm and 12 mm centerpieces, chosen dependent on loading concentration such that the anticipated absorbance signals at 280 nm (for low-affinity systems) or 230 nm (for high affinity systems) were as much as possible within the linear range of the optics. Where this could not be achieved, interference signals were taken for the determination of s_w. The c(s) distribution model in SEDFIT was applied with maximum entropy regularization and algebraic noise decomposition. This is appropriate despite the presence of a rapidly interacting system due to the property of interacting systems to exhibit diffusion similar to that of non-interacting species (Schuck, 2010), permitting the normal diffusional deconvolution by c(s) and precise modeling of the boundaries, with typical rms deviations of 0.005 fringes or 0.014 OD_{230} or better. Based on the faithful description of the measured boundaries by c(s), the second moment method to determine s_w is implicit in the integration of c(s), which therefore leads to rigorous s_w values (Schuck, 2003). The broad features of the measured boundaries and the rapid interaction kinetics indicates that models explicitly

describing chemical reactions kinetics coupled to sedimentation would not be useful. Next, the analysis of the $s_w(c)$ isotherm was carried out in SEDPHAT, using mass action law models described above. Small corrections for hydrodynamic interactions were applied with the factor $(1-k_s w)^{-1}$, where w is the total weight concentration of protein and k_s is the non-ideality coefficient assumed to be 0.01 ml/mg (Schuck, 2007), or where possible, refined in the fit to values up to 0.02 ml/mg. This amounts to maximum corrections at the highest concentrations of 2 – 3%. The species $s_{20,w}$ values were pre-determined from the isotherm analyses of molecules with high affinity at high concentrations and low affinity at low concentrations, respectively, and fixed to the values: $s_{1,\,KA2}$ = 3.91 S, $s_{2,\,KA2}$ = 5.82 S, $s_{1,\,GluR6\Delta2}$ = 3.72 S, $s_{2,\,GluR6\Delta2}$ = 5.79 S, $s_{1,\,GluR6\Delta2F58A}$ = 3.79 S, $s_{2,\,GluR6\Delta2F58A}$ = 5.79 S, and $s_{2,KA2\text{-}GluR6}$ = 5.54 S; the latter value was floated for the analysis of complex formation with high affinity. The s-value of the tetramer was estimated with the assumption that it has a similar frictional coefficient as the dimers, leading to ~ 9.1 S. Typical rms errors of the isotherm fits were 0.03 S or better.

SE experiments were conducted in 'aged' cell assemblies with 12 mm centerpieces and interference scans were corrected for systematic noise by subtraction of experimental water blanks. For the analysis of sedimentation equilibrium 15 – 24 absorbance or interference profiles from different rotor speeds and cells at different loading concentrations were globally fit in SEDPHAT with models for the radial distributions of ideally sedimenting species in chemical equilibrium. The model for the single-component samples of either the GluR6 or KA2 wild type and mutant ATDs was a

superposition of Boltzmann terms for monomer and dimer in chemical equilibrium, with the dimer concentration expressed *via* mass action law and the dimerization constant K_2

$$a_\lambda(r) = c_1(r_0)\varepsilon_\lambda d \exp\left[\frac{M_1^*(1-\bar{v}^*\rho)}{2RT}\omega^2\left(r^2 - r_0^2\right)\right] + K_2 c_1(r_0)^2 2\varepsilon_\lambda d \exp\left[\frac{2M_1^*(1-\bar{v}^*\rho)}{2RT}\omega^2\left(r^2 - r_0^2\right)\right]$$

(where *a* denotes the measured signal at wavelength λ, *r* the distance from the center of rotation, r_0 a reference radius *c* the molar concentration, ε the molar extinction, *d* the optical pathlength, M_1^* the monomer apparent molar mass on the scale of the partial-specific volume $\bar{v}^*$, ρ the solution density, *R* the gas constant, *T* the absolute temperature, and ω the rotor speed).

For analysis of GluR6 and KA2 mixtures, a model for mixed homo- and hetero-oligomer associations was implemented, with a radial distribution of the form

$$a_\lambda(r) = \sum_{i,j} K_{ij}\left(c_A(r_0)\right)^i\left(c_B(r_0)\right)^j\left(i\varepsilon_{A,\lambda} + j\varepsilon_{B,\lambda}\right)d \exp\left[\left(iM_A^* + jM_B^*\right)\frac{(1-\bar{v}^*\rho)}{2RT}\omega^2\left(r^2 - r_0^2\right)\right]$$

where the terms with (i=1, j=0) and (i=0, j=1) and K10 = K01 = 1 describe the radial distribution of the monomers, the terms with (i=2, j=0) and (i=0, j=2) describe the homo-dimers of each component formed via mass action law with binding constants K20 and K02, respectively, and a term with (i=1, j=1) describes the hetero-dimerization following mass action law with the hetero-dimerization constant K11. An additional term for dimerization of the hetero-dimers, with total equilibrium constant K22 , was added in the analysis of the interactions of wt GluR6 with KA2 shown in Figure S2C. The system of equations arising from the coupled chemical equilibria of all binding reactions was solved as described (Vistica et al., 2004). Where necessary, rotor-speed independent but radial-dependent, high spatial frequency systematic signal imperfections in the absorbance data

were accounted for as described previously (Vistica et al., 2004). In the global fit of the mixtures, the homo-dimerization constants, as well as the molar extinction and signal coefficients, were fixed to the best-fit values from the analysis of the individual components studied in parallel. Further, since the samples were derived from dilution series of a stock mixture, the soft mass conservation model allowed the molar ratio in each sample to be described by a single parameter linking the model from all cells (Vistica et al., 2004). For both single component samples and the mixture, the SE analysis led to root-mean-square deviations of between 0.002 and 0.005 OD, which compares well with the noise of data acquisition. Statistical uncertainties of the best-fit parameters were estimated using the projection method and F-statistics.

Cysteine cross linking and Western blots

Cells were harvested by centrifugation on the $4^{th}/5^{th}$ day post transfection and resuspended in 50 ml of 100 mM Tris pH 8.0, 200 mM NaCl buffer containing 2mM N-ethylmaleimide (NEM) for 15 minutes. The washed cell pellet was resuspended in 10ml lysis buffer (1.5% Triton, 100 mM Tris pH 8.0, 200 mM NaCl, 1x EDTA free protease inhibitor cocktail, 2mM NEM), mixed by end-to-end rotation overnight at 4º C, followed by a spin at 40K rpm for 45 minutes to pellet debris. The supernatant was loaded onto a 1ml StrepTactin sepharose high performance column (GE Biosciences) and the bound protein eluted using 2.5 mM desthiobiotin. The peak fraction was resolved on a 4-12.5% Bis-Tris gel, under non-reducing conditions for 90 minutes at 200 volts. The gel was electroblotted onto a PVDF membrane overnight at 35 volts in Tris/Glycine, 20% Methanol transfer buffer. Western analysis was run on a bench processing system

(Invitrogen) and the blots probed with anti-flag antibody (1:5000) & anti-strep antibody (1:2000) for detection of GluR6 and KA2 respectively.

Mutant cycle analysis

Domain 1

R6Δ2/KA2 F58A/Y57A
11 nM 1630 nM
Ω 1.18
R6F58A/KA2 R6Δ2/KA2Y57A
109 nM 140 nM

Domain 1 and Domain 2 site 2 (E156)

R6Δ2/KA2 R6Δ2/KA2Y57A/E156A
11 nM 380 nM
Ω 1.66
R6Δ2/KA2Y57A R6Δ2/KA2E156A
109 nM 23 nM

Domain 1 and Domain 2 site 3 (L163)

R6Δ2/KA2 R6Δ2/KA2Y57A L163A
11 nM 920 nM
Ω 0.88
R6Δ2/KA2Y57A R6Δ2/KA2L163A
109 nM 105 nM

Domain 1 and Domain 2 site 4 (S165/T168)

R6Δ2/KA2 R6Δ2/KA2Y57G--A
11 nM 1800 nM
Ω 0.82
R6Δ2/KA2Y57A R6Δ2/KA2G--A
109 nM 220 nM

R6 R1	KA2 R1	KA2 R2	Elution volume Peak 1 (ml)	Elution volume Peak 2 (ml)	%Change in Peak 2 area*	SV Kd (μM)	95% CI (μM)	ΔΔG (kcal/mol)
WT	---	---	13.27	NA	NA	0.25	0.205 – 0.302	
F58A	---	---	NA	14.80	NA	490	380 – 650	-4.41
---	WT	WT	NA	14.60	NA	350	320 – 385	
WT	WT	WT	13.16	14.88	-79	0.011	0.006 – 0.017	6.04
WT	Y57A	WT	13.17	14.77	-76	0.140	0.112 – 0.175	-1.48
F58A	WT	WT	13.17	14.79	-78	0.109	0.096 – 0.121	-1.35
F58A	Y57A	WT	13.38	14.80	-62	1.63	1.57 – 1.70	-2.91
WT	Y57A	E156A	13.19	14.59	-38	0.38	0.33 – 0.43	-3.03
F58A	Y57A	E156A	NA	13.58	+114	2.0	0.18 – 2.27	-0.43
WT	WT	E156A	13.09	14.36	-57	0.023	0.013 – 0.039	
F58A	WT	E156A	13.28	14.46	-65	ND		
WT	Y57A	L163A	13.25	14.70	-25	0.92	0.81 – 1.06	-2.58
F58A	Y57A	L163A	NA	13.80	+114	6.7	6.4 – 7.1	-3.73
WT	WT	L163A	13.16	14.83	-63	0.105	0.089 – 0.125	-1.31
F58A	WT	L163A	13.33	14.85	-62	ND		
WT	Y57A	I164A	13.26	14.80	+3	> 200 μM		
F58A	Y57A	I164A	NA	14.80	+110	> 200 μM		
WT	WT	I164A	13.27	14.75	+2	> 200 μM		
F58A	WT	I164A	NA	14.70	+105	ND		
WT	WT	L163A/I164A	13.27	14.88	+11	> 200 μM		
F58A	WT	L163A/I164A	NA	14.78	+106	ND		
WT	Y57A	E156A/AA	13.22	14.77	+4	> 200 μM		
F58A	Y57A	E156A/AA	NA	14.82	+101	> 200 μM		
WT	WT	E156A/AA	13.24	14.81	+2	> 200 μM		
F58A	WT	E156A/AA	NA	14.82	+116	> 200 μM		
WT	Y57A	- - G- -A	ND	ND	ND	1.8	1.3 – 2.4	-2.97
F58A	Y57A	- - G- -A	ND	ND	ND	13.0	10 – 15	-4.12
WT	WT	- - G- -A	ND	ND	ND	0.22	0.19 – 0.26	-1.74
F58A	WT	- - G- -A	ND	ND	ND	ND		
WT	Y57A	AAG- -A	13.27	14.84	+5	ND		
F58A	Y57A	AAG- -A	NA	14.83	+106	ND		
WT	Y57A	E156A/AAG- -A	13.26	14.85	+12	ND		
F58A	Y57A	E156A/AAG- -A	NA	14.83	+115	ND		
WT	WT	E156A/AAG- -A	13.24	14.95	+5	ND		
F58A	WT	E156A/AAG- -A	NA	14.89	+107	ND		

Table S1. For analysis of GluR6Δ2 and KA2 ATDs by SEC- UV/RI/MALS the elution volumes are given for peaks 1 and 2, corresponding to dimers and monomers, together with the change in area for peak 2 calculated with reference to the signal for KA2 injected alone. Depletion of peak 2 indicates formation of heterodimers; the extent of depletion is proportional to heterodimer affinity. An increase in peak 2 amplitude occurs when a KA2 mutant with reduced heterodimer affinity is mixed with the GluR6Δ2F58A

mutant which is incompetent to form homodimers at the loading concentration of 2 mg/ml used for these experiments. Dimer K_d values are reported for data from sedimentation velocity experiments, together with the 95% confidence intervals. Where appropriate ΔΔG values for changes in binding energy are calculated with respect to the reference values of 250 nM for GluR6Δ2 homodimers, 350 μM for KA2 homodimers, and 11 nM for the GluR6Δ2/KA2 heterodimer.

NA	: Not applicable
ND	: Not determined
E156A/AA	: E156A/L163A/I164A
- - G- -A	: S165G/T168A
AAG- -A	: L163A/I164A/ S165G/T168A
E156A/AAG- -A	: E156A/ L163A/I164A/ S165G/T168A
*	: (-) indicates depletion, (+) indicates increase in peak 2 area

SUPPLEMENTAL REFERENCES

Adams, P. D., Afonine, P. V., Bunkoczi, G., Chen, V. B., Davis, I. W., Echols, N., Headd, J. J., Hung, L. W., Kapral, G. J., Grosse-Kunstleve, R. W., et al. (2010). PHENIX: a comprehensive Python-based system for macromolecular structure solution. Acta Crystallogr D Biol Crystallogr 66, 213-221.

CCP4 (1994). The CCP4 suite: programs for protein crystallography. Acta Crystallog sect D 50, 760-763.

Davis, I. W., Murray, L. W., Richardson, J. S., and Richardson, D. C. (2004). MOLPROBITY: structure validation and all-atom contact analysis for nucleic acids and their complexes. Nucleic Acids Res 32, W615-619.

DeLano, W. L. (2002). The PyMOL Molecular Graphics System (Palo Alto, CA, USA: DeLano Scientific).

Durchschlag, H. (1989). Determination of the partial specific volume of conjugated proteins. Colloid and Polymer Science, 1139-1150.

Gorrec, F. (2009). The MORPHEUS protein crystallization screen. J Appl Cryst 42, 1035-1042.

Kleywegt, G. J., Zou, J. Y., Kjeldgaard, M., and Jones, T. A. (2001). Around O, In Crystallography of Biological Macromolecules (Dordrecht: Kluwer Academic Publishers), pp. 353-356.

Kumar, J., and Mayer, M. L. (2010). Crystal Structures of the Glutamate Receptor Ion Channel GluK3 and GluK5 Amino-Terminal Domains. J Mol Biol 404, 680-696.

Kumar, J., Schuck, P., Jin, R., and Mayer, M. L. (2009). The N-terminal domain of GluR6-subtype glutamate receptor ion channels. Nat Struct Mol Biol 16, 631-638.

Painter, J., and Merritt, E. A. (2006). Optimal description of a protein structure in terms of multiple groups undergoing TLS motion. Acta Crystallogr D Biol Crystallogr 62, 439-450.

Ramachandran, G. N., Ramakrishnan, C., and Sasisekharan, V. (1963). Stereochemistry of polypeptide chain configurations. J Mol Biol 7, 95-99.

Schroder, G. F., Levitt, M., and Brunger, A. T. (2010). Super-resolution biomolecular crystallography with low-resolution data. Nature 464, 1218-1222.

Schuck, P. (2003). On the analysis of protein self-association by sedimentation velocity analytical ultracentrifugation. Anal Biochem 320, 104-124.

Schuck, P. (2007). Sedimentation velocity in the study of reversible multiprotein complexes, In Protein Reviews, P. Schuck, ed., pp. 469-518.

Schuck, P. (2010). Diffusion of the reaction boundary of rapidly interacting macromolecules in sedimentation velocity. Biophys J 98, 2741-2751.

Vistica, J., Dam, J., Balbo, A., Yikilmaz, E., Mariuzza, R. A., Rouault, T. A., and Schuck, P. (2004). Sedimentation equilibrium analysis of protein interactions with global implicit mass conservation constraints and systematic noise decomposition. Anal Biochem 326, 234-256.

Figure S1. Control of GluR6 aggregation by an engineered glycan wedge, Related to Figure 1.

(A) Size exclusion chromatography (SEC-UV/RI/MALS) analysis for wildtype GluR6 ATD at pH 7.4 showing the broad elution profile and shift in mass from apparent tetramer to dimer on the trailing edge. (B) Sedimentation velocity analysis for homomeric wildtype GluR6 at pH 7.4 reveals a reversible, concentration dependent formation of multiple high MW species with S-values much larger than predicted for dimers (5.6-5.8 S) or tetramers (9.1 S). (C) Crystal lattice for wildtype GluR6 ATD (PDB 3H6G) with domains R1 and R2 colored green and blue respectively; orange spheres indicate the position of Ala213; the view down the *c* axis of the $P6_1$ lattice illustrates spiral arrays mediated by domain R2 contacts which potentially could lead to the reversible aggregation of wildtype GluR6 ATD. (D) cartoon showing a hypothetical mechanism for formation of high order oligomers by wildtype GluR6 ATD dimers in solution. (E) cartoon showing isolated GluR6 ATD dimer assemblies produced by an engineered glycan wedge on the solvent exposed face of domain R2 for the A213N/G215S (Δ1) and G215N/M217T (Δ2) mutants. (F) Crystal lattice for the GluR6 Δ1 mutant using the same coloring scheme, but with the mutant NAG residue at position 213 shown as orange spheres; the view down the down the *c* axis of the I4 lattice reveals that the glycan wedge projects into a solvent channel running down the 4-fold axis of symmetry.

Figure S2. The GluR6Δ1 glycan wedge mutant used for crystallization has identical solution behavior to GluR6Δ2, Related to Figures 1 and 2.

(A) Superimposed gel permeation chromatography profiles for the GluR6Δ1 and KA2 ATDs when the proteins were injected separately; analysis by SEC-UV/RI/MALS (red data points) revealed elution with mass values corresponding to dimers and monomers respectively. (B) When the two proteins were mixed at approximately equal concentrations prior to injection, the amplitude of the dimer peak increased, with a corresponding decrease in the monomer peak, indicating formation of GluR6/KA2 heterodimers; dashed lines show data from B scaled by 50% to account for the dilution factor when the samples were mixed. The profiles illustrated here are indistinguishable from those obtained with the GluR6Δ2 mutant.

Figure S3. Formation of GluR6/KA2 ATD tetramers, Related to Figure 2

(A) SEC profiles for a mix of wt GluR6 + KA2 ATDs at pH 7.4, black line; wt GluR6 alone, blue dashed line; and GluR6Δ2 + KA2, red dashed line. (B) Sedimentation velocity analysis for an equimolar mix of wildtype GluR6 and KA2 ATDs reveals three peaks at S values of 3.7, 5.6 and 6.9 at a loading concentration of 5.5 μM, corresponding well to the S values of monomers, homo- and hetero-dimers, and a reaction boundary from transient formation of tetramers with an S value of 9.1 S. (C) Sedimentation equilibrium analysis for the same mix, fit with a model for monomer-dimer-tetramer equilibrium, in which the K_d for formation of GluR6 homodimers and GluR6/KA2 heterodimers were constrained to values measured in experiments with the GluR6Δ2 mutant. The lower panel show residuals for a single cell from a global fit to data for 3 loading concentrations each run at three speeds (6,500 rpm, 10,000 rpm, and 16,000 rpm). Although this model fits the data well, with a K_d of 3.5 μM for formation of

tetramers from pairs of heterodimers, this value is likely to be underestimated due to the unaccounted for contributions of poorly characterized wtR6 homo-oligomers which inevitably will be formed in chemical equilibrium with the pool of free wtR6. Application of the same model to the sw isotherm derived from the data of panel B also leads to an excellent fit with a similar K_d of 6.2 μM for formation of tetramers from pairs of heterodimers (data not shown).

Figure S4. Electron density maps for the domain R1 and domain R2 interfaces in GluR6/KA2 heterodimers, Related to Figure 3 and Figure 4

(A and B) Stereoview of the GluR6Δ1/KA2 heterodimer domain R1 dimer interface viewed parallel to molecular axis of 2-fold pseudosymmetry; the 2 mFo-DFc electron density maps are contoured at 1.2 σ; ribbon diagrams for the GluR6 and KA2 are subunits colored green and red respectively, with side chains colored wheat and teal. The view in A shows the interaction of KA2 Tyr57 with the GluR6 subunit; the view in B is rotated by 180° and shows the interaction of GluR6 F58 with the KA2 subunit. (C) Stereoview of the GluR6/KA2 heterodimer domain R2 dimer interface viewed parallel to molecular axis of 2-fold pseudosymmetry using the same coloring scheme and map contours. (D) Stereoview of the domain R2 dimer interface showing interactions between the GluR6 and KA2 subunits, with hydrogen bonds drawn as dashed lines, and residues in VDW contact indicated by transparent CPK spheres.

Figure S5. Assays for heterodimer formation by GluR6 and KA2 ATD mutants , Related to Figure 5

(A) SEC-UV/RI/MALS analysis for the KA2 C64S/C315S double mutant injected alone (dashed blue line), or as an equimolar mix with either GluR6Δ2 (solid black line) or the GluR6Δ2 F58A mutant (dashed black line); depletion of the KA2 monomer peak indicates heterodimer formation with both GluR6Δ2 and GluR6Δ2 F58A. (B) A similar analysis for the KA2 E156A/L163A/I164A triple mutant two well resolved peaks for the GluR6Δ2 plus KA2 mutant mix, corresponding to GluR6Δ2 dimers and KA2 mutant monomers, with an increase in the monomer peak for the GluR6Δ2 F58A plus KA2 mutant mix, indicating no interaction between the GluR6 and KA2 ATDs. (C) Isotherms of weighted-average sedimentation coefficients for mixtures of GluR6Δ2 and the indicated KA2 mutants, fit with a monomer-dimer model for which the heterodimer K_d spans a > 500-fold range, from 30 nM for E156A to undetectable dimerization for the Y57A/E156A/L163A/I164A quad mutant. (D) Monomer, homodimer and heterodimer species, plotted as a function of total protein concentration for the GluR6Δ2/KA2 Y57A/L163A mutant, calculated from the fit shown in panel C.

Figure S6. Crystal packing of the wildtype GluR6/KA2 ATD heterotetramer, Related to Figure 6

(A) The unit cell is drawn in black and viewed down the *b* axis. The 10 chains in one asymmetric unit are colored green for GluR6 and red for KA2 subunits respectively. The 10 protomers are arranged as two heterotetramers, with a third identical tetramer created by crystal symmetry operations for the remaining heterodimer. (B) Electron density map (2mFo-DFc contoured at 1.2 σ) for one of the GluR6/KA2 heterotetramers with a Cα

trace for the GluR6 (green) and KA2 (red) subunits; the labels R1, R2, R1□and R2□ indicate the location of domains 1 and 2 in the two GluR6 subunits.

Supplemental Figure 1

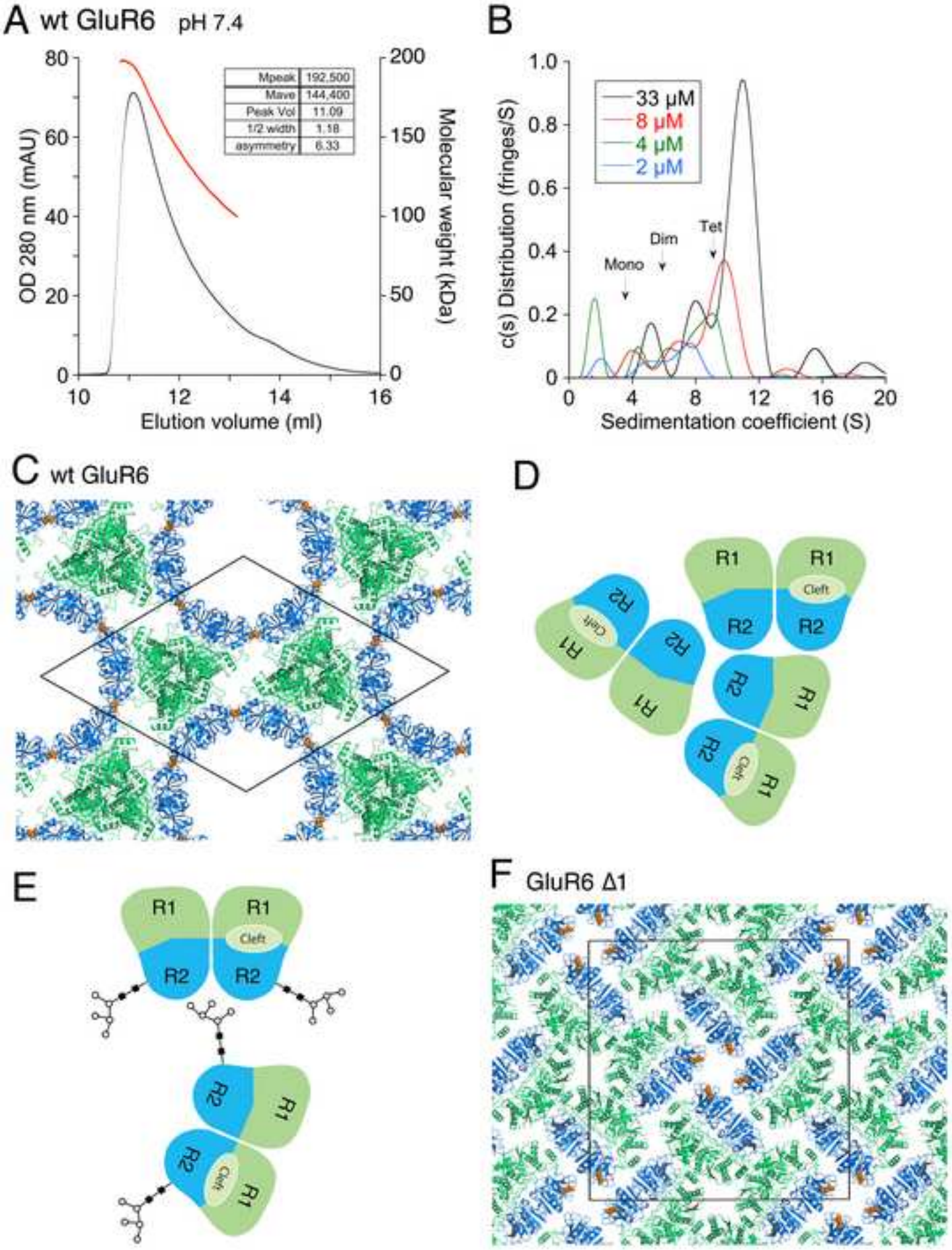

Supplemental Figure 2

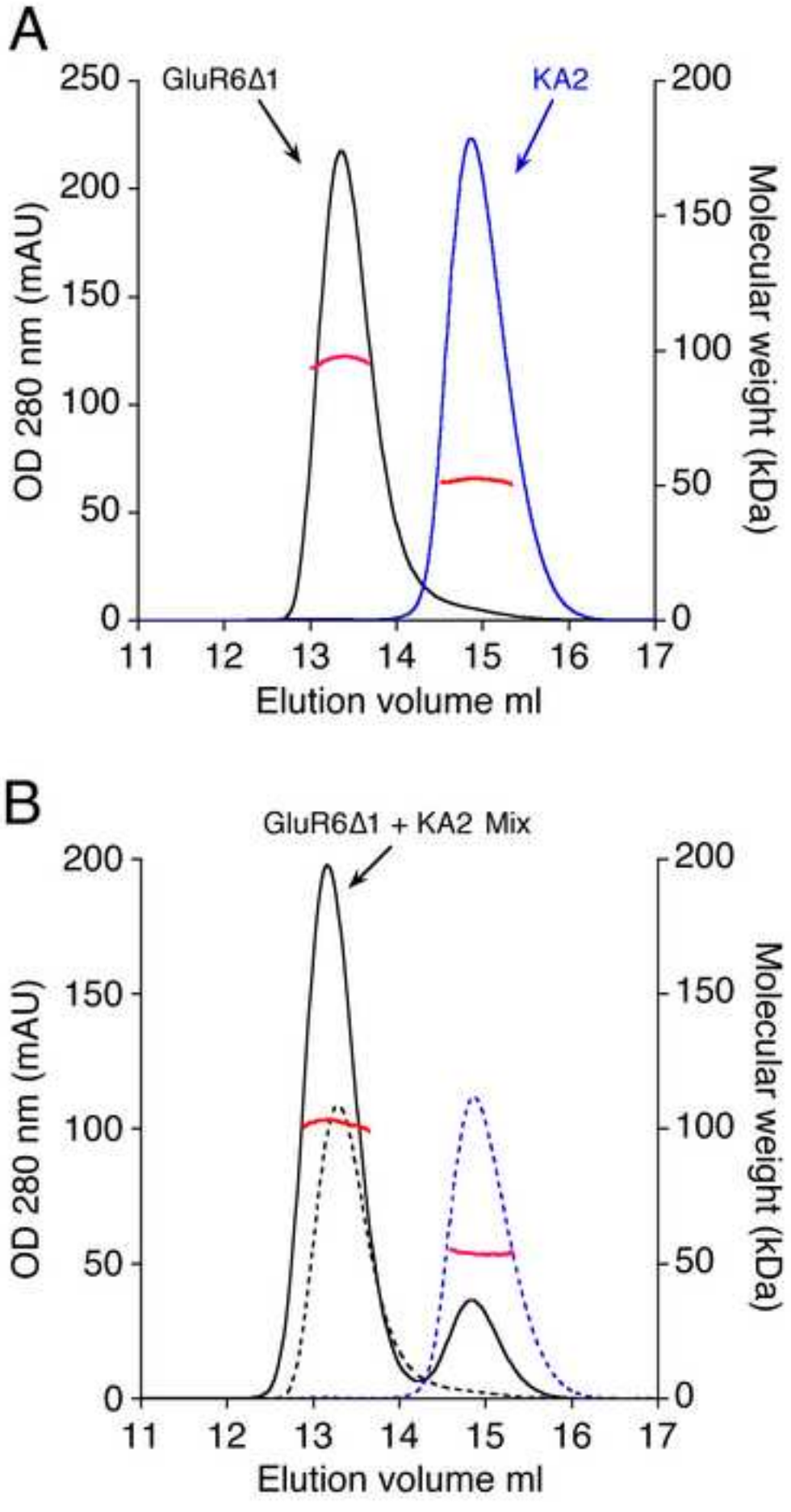

Supplemental Figure 3

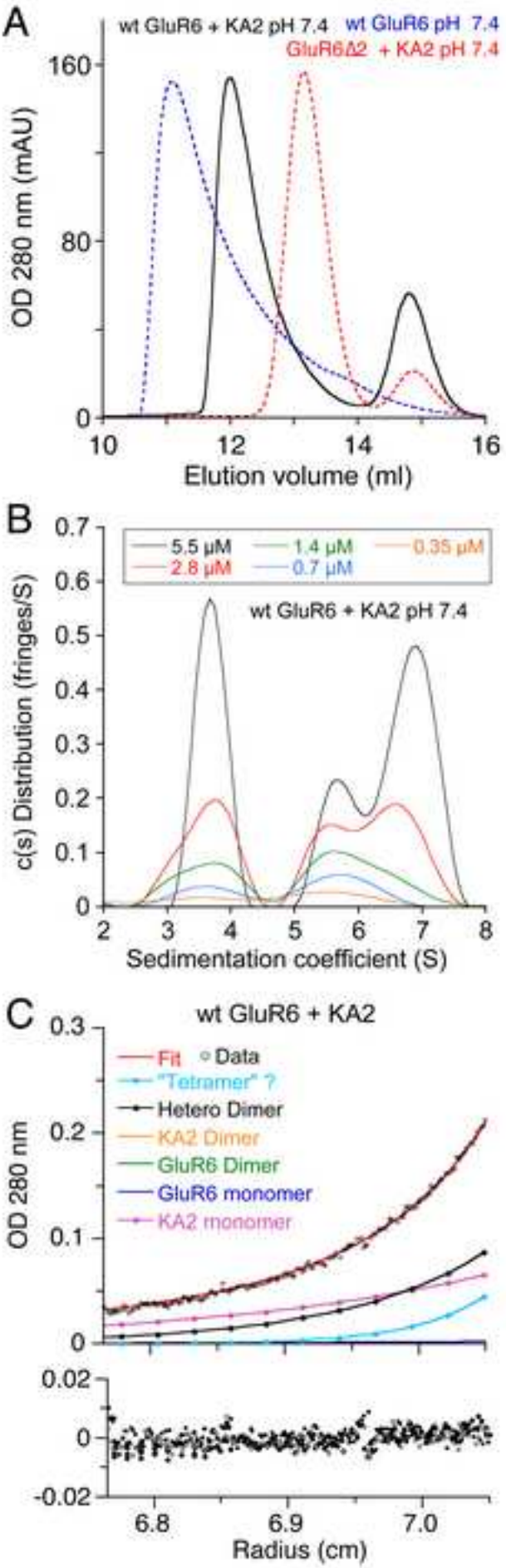

Supplemental Figure 4

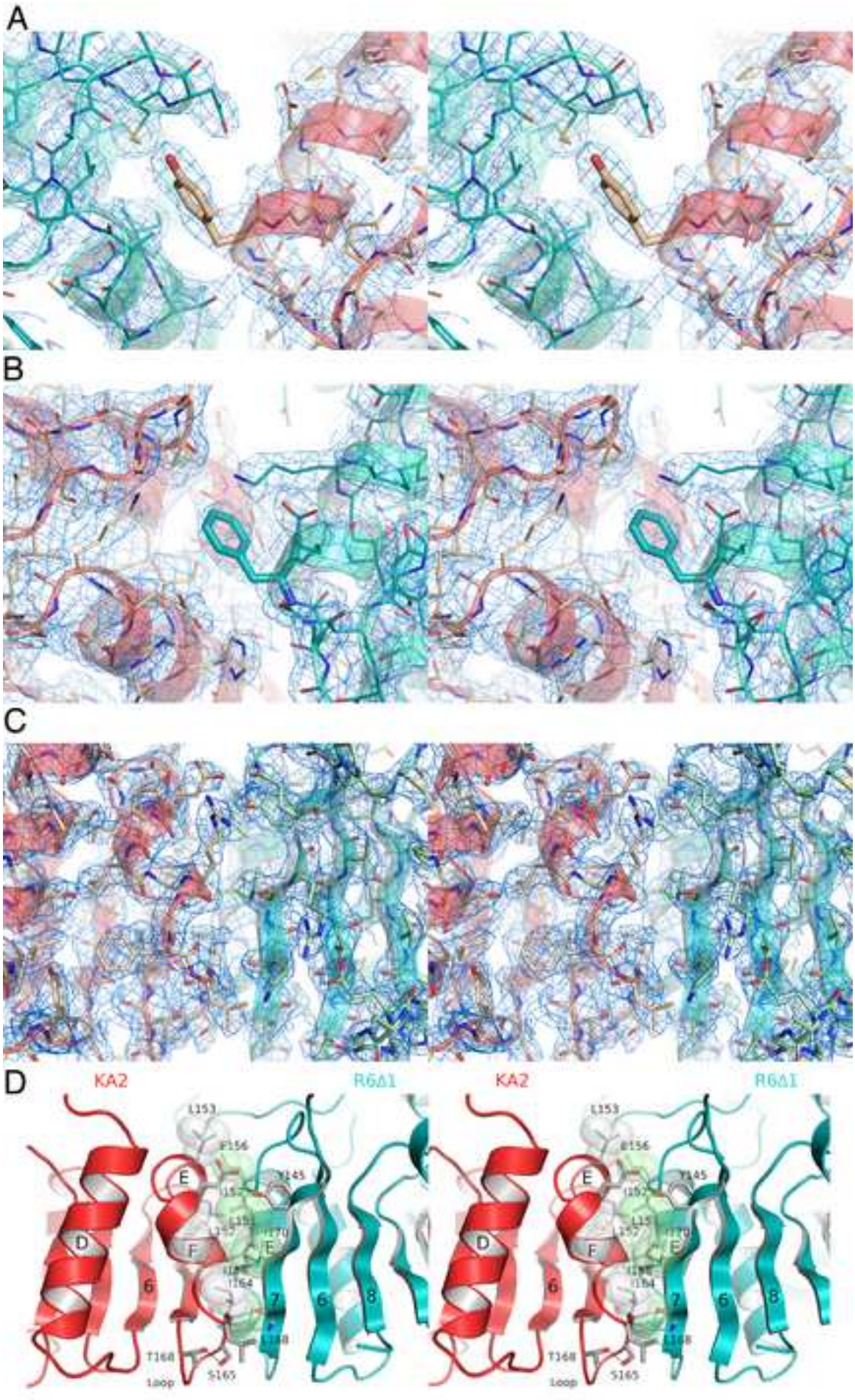

Supplemental Figure 5

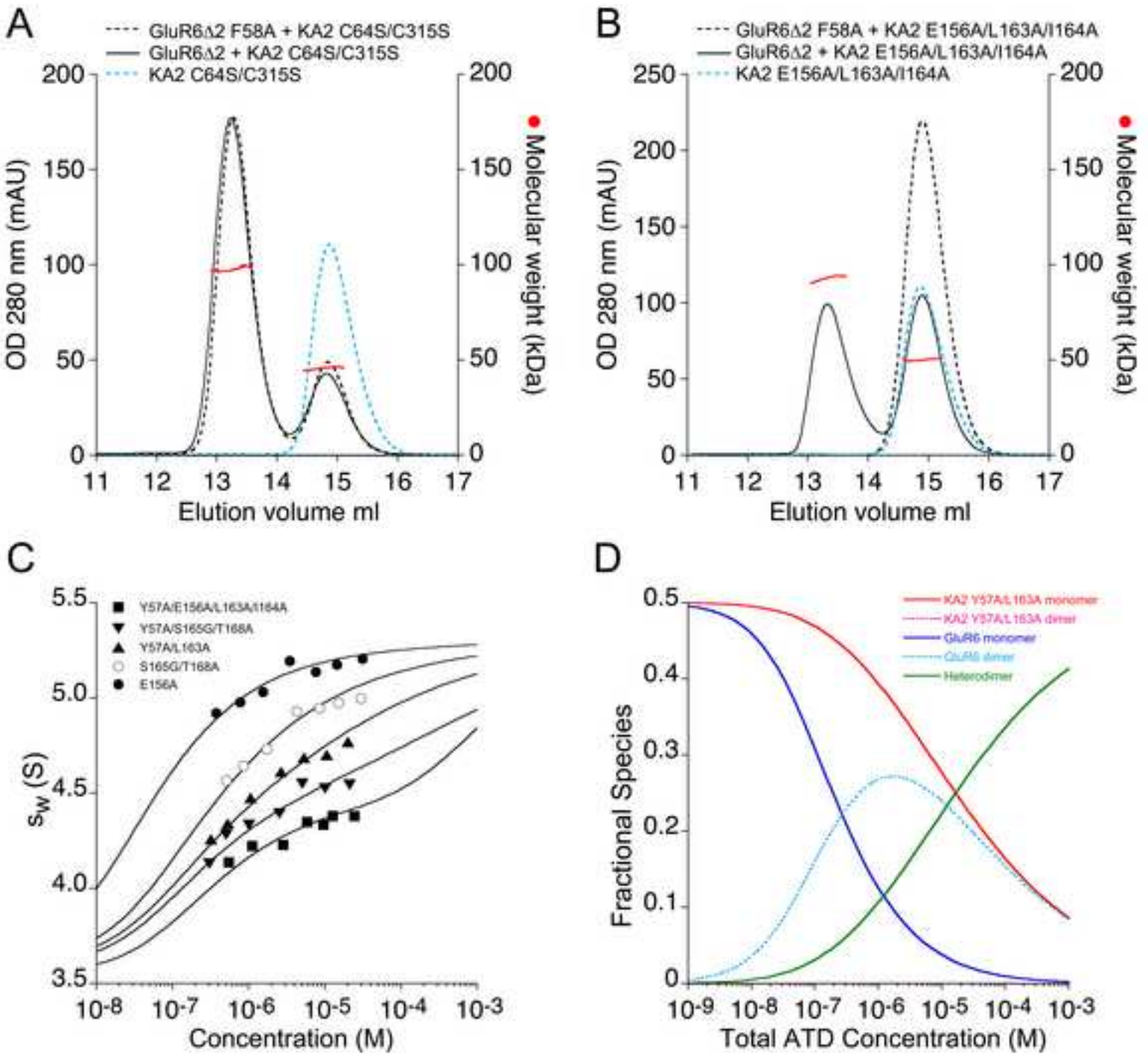

Supplemental Figure 6